

Assimilation of land surface temperature into the land surface model JULES with an ensemble Kalman filter

D. Ghent,¹ J. Kaduk,¹ J. Remedios,² J. Ardö,³ and H. Balzter¹

Received 21 April 2010; revised 15 June 2010; accepted 27 July 2010; published 7 October 2010.

[1] Land surface models have uncertainties due to their approximation of physical processes and the heterogeneity of the land surface. These can be compounded when key variables are inadequately represented. Land surface temperature (LST) is critical as it forms an integral component in the surface energy budget, water stress evaluation, fuel moisture derivation, and soil moisture–climate feedbacks. A reduction in the uncertainty of surface energy fluxes, and moisture quantification, is assumed to be achievable by constraining simulations of LST with observation data. This technique is known as data assimilation and involves the adjustment of the model state at observation times with measurements of a predictable uncertainty. In this paper, the validity of LST simulations in a regionalized parameterization of the land surface model Joint UK Land Environment Simulator (JULES) for Africa is assessed by way of a multitemporal intercomparison study with the Moderate Resolution Imaging Spectroradiometer (MODIS), the Advanced Along Track Scanning Radiometer (AATSR), and the Spinning Enhanced Visible and Infrared Imager (SEVIRI) thermal products, with a two-thirds reduction in model bias found when soil properties are reparameterized. A data assimilation experiment of SEVIRI LST into the JULES model via an ensemble Kalman filter shows an improvement in the modeled LST, soil moisture, and latent and sensible heat fluxes. This paper presents the first investigation into reducing the uncertainty in modeling energy and water fluxes with the United Kingdom's most important land surface model, JULES, by means of data assimilation of LST.

Citation: Ghent, D., J. Kaduk, J. Remedios, J. Ardö, and H. Balzter (2010), Assimilation of land surface temperature into the land surface model JULES with an ensemble Kalman filter, *J. Geophys. Res.*, 115, D19112, doi:10.1029/2010JD014392.

1. Introduction

[2] Land surface models are mathematical representations of the biophysical processes that constitute the terrestrial biosphere. They are crucial elements of general circulation models (GCMs), since they determine the surface radiative properties and the surface to atmosphere fluxes of heat, water and carbon; influencing cloud cover, precipitation, and atmospheric chemistry. However, much variation exists in their parameterization, representation of biophysical processes, and as a result of the heterogeneity of the land surface; leading to uncertainty in how climate change influences the terrestrial biosphere, and how the land surface may evolve in the future. Improvements can be made by integrating additional data into these models; a technique known as data assimilation. While field measurements can provide accurate constraints to models, their limited geo-

graphical extent reduces their effectiveness, whereas remotely sensed data from Earth observation (EO) satellites can overcome this limitation thereby providing the most realistic source of data at appropriately fine temporal resolution over large geographical regions.

[3] Data assimilation involves adjusting the model state with external measurements of established uncertainty at regular intervals. With the inherent uncertainty in model predictions, data assimilation represents a process of minimizing the errors in the model physics through the updating of the model state variables at each time step when observations become available. Both the model uncertainty and the observation uncertainty play significant roles in the determination of the correction to be applied to the state variable. Where the observation data values are more reliable the model estimates are adjusted to more closely correspond to these observations.

[4] Several assimilation techniques exist, including the three-dimensional variational (3DVAR) scheme, and the Kalman filter method and its variants. The difference between these is in the evolution of the error structure, and the methodology for solving the analysis update equation. The Kalman filter provides the optimum linear sequential assimilation solution based on model and observation uncertainties [*Gelb,*

¹Department of Geography, University of Leicester, Leicester, UK.

²Department of Physics and Astronomy, University of Leicester, Leicester, UK.

³Department of Earth and Ecosystem Sciences, Lund University, Lund, Sweden.

1974], and is designed to apply this prior knowledge of the uncertainties to achieve the optimum correction to be applied to the model estimation. To cope with nonlinear assimilation a variant called the extended Kalman filter (EKF) was developed. An alternative to this is the ensemble Kalman filter (EnKF) [Evensen, 2003], which employs a Monte Carlo approach to avoid the computationally expensive integration of the state error covariance matrix; and compared with the EKF is more robust and flexible in covariance modeling [Reichle et al., 2002].

[5] Previous implementations of the EnKF have indicated this technique to be a beneficial solution for updating state variables with observation measurements. For instance, Huang et al. [2008] reported a 1 K improvement in the estimates of soil temperature when satellite land surface temperature (LST) products were assimilated at observation times. Quaipe et al. [2008] assimilated canopy reflectance into a simple carbon pool and box model, and found significant improvements in the estimation of gross primary production. Pipunic et al. [2008] assimilated LST products, and both latent heat and sensible heat products. They found predictions of latent and sensible heat were improved under both assimilation scenarios. Furthermore, they found that assimilation of higher temporal source data resulted in improved predictions compared with lower temporal source data.

[6] In this study, we investigated the feasibility of assimilating LST into the Joint UK Land Environment Simulator (JULES) land surface model, which is the community version of the UK Met Office's Met Office Surface Exchange Scheme (MOSES) scheme. Although simulations from land surface models may well be reasonably representative of real values, during long modeling runs considerable deviation can result [Huang et al., 2008]. Constraining these simulations with observation data is therefore a desirable objective.

[7] LST is the radiative skin temperature of the land. It is derived from solar radiation and influences the partitioning of energy into ground, sensible, and latent heat fluxes. Being an important component of the surface energy budget it is therefore of significant value in validating and constraining land surface models. It is influenced by various surface-atmosphere boundary conditions, such as albedo, and precipitation [Huang et al., 2008]; and is more closely related to the physiological activities of leaves than air temperature [Sims et al., 2008]. Furthermore, differences between the air temperature and surface temperature of dry ground can be as much as 20°C [Byrne et al., 1979].

[8] The importance of LST in applications such as vegetation water stress monitoring, as a result of its close relationship to vapor pressure deficit [Hashimoto et al., 2008]; and surface energy balance assessment [Pinheiro et al., 2006], is well documented. Additionally, LST has an important role to play in the fire regime. It has been argued in previous studies [Sandholt et al., 2002; Snyder et al., 2006] that the ratio between the normalized difference vegetation index (NDVI) and LST can be expressed as a surface dryness index representing live fuel moisture content (FMC), which is a critical variable in the prediction of fire occurrence and propagation.

[9] A primary use of LST data derived from EO satellites has been in the validation/calibration of other LST data sets

[Noyes et al., 2006; Trigo et al., 2008a]. However, maybe in recognition of the important role LST has to play in land surface modeling, much recent work with satellite derived LST data has focused on this data being used as the source of observations to constrain models. Numerous studies have investigated the use of LST observations from satellite in model simulations. Bosilovich et al. [2007], for example, employed the 3DVAR assimilation method to assimilate LST into the National Center for Atmospheric Research (NCAR) Community Land Model. Margulis and Entekhabi [2003] also used a variational assimilation technique to optimize the water and energy budgets of a 1-D model. As for LST validation studies, both Ge et al. [2008] and Jin et al. [1997] compared land surface model LST simulations with remote sensing observations. These studies illustrated the importance of LST in the surface energy balance representation in biophysical models, and argued how improvements can be made with the utilization of satellite observations. A similar study involving JULES is thus a valuable objective. This study however, is the first to both attempt to validate the simulation of LST from a land surface model with satellite derived LST data from multiple sources, and to assimilate the most spatially and temporally appropriate product into the model using a sequential assimilation method, such as the EnKF. The ultimate aim of this study is to investigate the impact of a better representation of LST in the land surface model both on surface energy fluxes and biogeochemical cycles.

[10] Whereas many previous assimilation studies have successfully improved the estimations from simple biosphere models, few such as the assimilation of NDVI data into the Organizing Carbon and Hydrology In Dynamic Ecosystems Environment (ORCHIDEE) land surface model [Vivoy et al., 2001] have attempted to integrate satellite data into more complex biophysical and biogeochemical models. The current study represents a first investigation at sequential assimilation with the EnKF into the land surface model employed within the UK Met Office's Unified Modeling System. This paper will describe this land surface model and the assimilation methodology applied (section 2); and will present the results of the intercomparison of the model with remote sensing products, and of the assimilation of the observations into the model (section 3). Potential deficiencies in the existing state variable estimation will be discussed and improvements through assimilation will be analyzed (section 4).

2. Materials and Methods

2.1. Model Description

[11] JULES is based on the MOSES system, which was developed to calculate the surface-to-atmosphere fluxes of heat and water when coupled to the Hadley Centre's General Circulation Model (GCM), and is described in detail by Cox et al. [1999]. It is a terrestrial grid box model driven by meteorological data and features a fine temporal resolution to characterize the diurnal cycle, updating the state variables at intervals typically of 30 or 60 min. Additionally, it is coupled to a dynamic global vegetation model called Top-down Representation of Interactive Foliage and Flora Including Dynamics (TRIFFID) which adopts a heuristic modeling approach for determining vegetation distribution

and carbon storage. A feature of the model is that for the duration of the model run biophysical parameters remain constant.

[12] Each grid box is represented as a composite of nine surface “tiles.” These consist of five plant functional types (PFTs): broadleaf trees, needleleaf trees, C_3 grasses, C_4 grasses, and shrubs; and four nonvegetation types: urban, inland water, bare soil and ice. The subsurface of each grid box is profiled into four soil layers, with each layer homogeneous within a grid box. Soil thermal characteristics are functions of soil moisture, with diffusive heat exchanges between layers. Using the mean heat and water fluxes over the time step, prognostic soil fields are updated from values for the previous time step [Cox *et al.*, 1999; Smith *et al.*, 2006]. Dynamic vegetation structure is simulated as the density of carbon and fractional cover of the five PFTs, with modified Lotka-Volterra equations determining competitive advantages between PFTs as described by Hughes *et al.* [2006].

[13] Unlike single-source models, which can produce model errors in their predictions of surface heat fluxes in mixed canopy/soil surfaces [Kustas and Norman, 1999], JULES explicitly treats the energy exchanges between each tile and the overlying atmosphere; with the surface energy balance equation for each tile, as defined by Cox *et al.* [1999], given by

$$SW_N + LW_1 - \sigma T_s^4 = H + LE + G_0 \quad (1)$$

where T_s is the surface temperature, σ is the Stefan–Boltzmann constant, SW_N is the net downward short wave radiation derived from the surface albedo, LW_1 is the downward long wave radiation, H is the sensible heat flux, LE is the latent heat flux, and G_0 is the heat flux into the ground. The grid box LST is a sum of the surface temperatures of each tile multiplied by their respective fractional covers within the grid box.

[14] The surface temperature T_s is a critical variable in the derivation of sensible heat flux H (equation (2)), and latent heat flux LE (equation (3)). The sensible heat flux is calculated using the temperature gradient between the surface and reference height z_1 above the surface:

$$H = \frac{\rho c_p}{r_a} \left(T_s - T_1 \frac{g}{c_p} z_1 \right) \quad (2)$$

where ρ is the surface air density, c_p is the specific heat capacity of the air, r_a is the aerodynamic resistance, g is the acceleration due to gravity, and T_1 is the air temperature at reference height z_1 . The latent heat flux is similarly derived using the humidity gradient between the surface and atmospheric reference height z_1 :

$$LE = \Psi \frac{L\rho}{r_a} (q_{sat}(T_s) - q_1) \quad (3)$$

whereby LE is driven by evapotranspiration (ET), with Ψ being a factor determined from the proportions of canopy evaporation, bare soil evaporation, transpiration by vegetation, and sublimation from snow. L is the latent heat of vaporization of water, $q_{sat}(T_s)$ is the saturated specific humidity at surface temperature T_s , and q_1 is the specific

humidity at reference height z_1 . Within the soil hydrology component of the model, total unfrozen soil moisture content M within each layer is given by equation (4), in which the surface soil moisture is incremented according to equation (5):

$$M = \rho_w \Delta z \Theta_u \quad (4)$$

$$\frac{dM_1}{dt} = P_f + S_m - Y_s - W_1 - \rho(1 - f_a) \{ q_{sat}(T_s) - q_1 \} \cdot \left\{ \frac{(1 - \nu)\beta(\Theta_1)}{r_a + r_{ss}} + \frac{e_1 \nu}{r_a + r_c} \right\} \quad (5)$$

where ρ_w is the density of water, Δz is the depth of the soil layer, and Θ_u is the volumetric concentration of unfrozen soil moisture. P_f is the throughfall precipitation, S_m is snowmelt, Y_s is surface runoff, W_1 is the diffusive water flux flowing out to the layer below, f_a is the wet canopy fraction of the grid box, ν is the vegetated fraction of the grid box, $\beta(\Theta_1)$ is the soil moisture availability factor with volumetric soil moisture concentration Θ_1 in the topsoil layer, e_1 is the fraction of the transpiration extracted from the topsoil layer; and r_{ss} and r_c are a fixed soil surface resistance and the canopy resistance, respectively. For more comprehensive detail regarding the soil thermodynamic and hydrology components of the model, these are described by Cox *et al.* [1999].

2.2. Study Area

[15] For this investigation the study region was Africa, chosen in order to assess the benefits of LST assimilation over a large geographical area at a fine temporal resolution. Africa has a strong wet and dry seasonality, and is an important component in the global carbon cycle; yet this continent remains the least studied [Intergovernmental Panel on Climate Change, 2007], even though climate scenarios for Africa remain highly uncertain [Williams *et al.*, 2007]. During the 20th Century Africa experienced an overall warming. With warming expected to accelerate here in most scenarios [Hulme *et al.*, 2001], improved quantification of the surface to atmosphere heat and water fluxes through data assimilation offers the prospect of improving confidence in climate predictions for this region. Furthermore, the simulation of realistic fire disturbance regimes with biophysical and biogeochemical models, by applying improved estimations of FMC, is a prerequisite for reducing the uncertainty of the African carbon cycle. Since the observation network around Africa is relatively sparse only EO data represents a feasible option for constraining model estimates.

2.3. Experimental Setup

[16] For this study, JULES version 2.1 was run at an hourly time step at $1^\circ \times 1^\circ$ spatial resolution. Meteorological input data were taken from 6-hourly National Centers for Environmental Prediction (NCEP) reanalysis data sets [Kalnay *et al.*, 1996]. However, caution has been advocated in the use of NCEP precipitation data [Ichii *et al.*, 2005], so calibration with monthly Tropical Rainfall Measuring Mission (TRMM) precipitation data [Kummerow *et al.*, 1998] was therefore applied according to the method used by Sheffield *et al.* [2006] and Weber *et al.* [2009], in which

the 6-hourly NCEP values are scaled to match the monthly TRMM values as follows:

$$\text{Calibrated NCEP}_{6\text{hr}} = \frac{\text{TRMM}_{\text{monthly}}}{\text{NCEP}_{\text{monthly}}} \times \text{NCEP}_{6\text{hr}} \quad (6)$$

[17] Land cover change was not considered in this experiment, since the duration of the model run was too short to trigger significant vegetation–climate feedbacks as a result of changes to vegetation distribution. The geographical distribution of the JULES tiles was therefore determined from the seventeen International Geosphere–Biosphere Programme (IGBP) land cover classes, which are available in a $1^\circ \times 1^\circ$ gridded file from the International Satellite Land Surface Climatology (ISLSCP) Initiative II data collection, by applying the linear mapping algorithm of *Dunderdale et al.* [1999], rather than being simulated by TRIFFID. JULES was spun up until the soil thermal and hydrologic properties, and the modeled carbon cycle, were equilibrated with the climate forcing. This equilibrium state is used as the initial condition for the main run, and limits anomalous responses at the beginning of the simulation.

[18] LST simulated by JULES was compared during March, June, September, and December 2006 with three widely used thermal satellite products: the Advanced Along Track Scanning Radiometer (AATSR); the Moderate Resolution Imaging Spectroradiometer (MODIS); and the Spinning Enhanced Visible and Infrared Imager (SEVIRI). The choice of 4 distinct months enabled any seasonal effects to be highlighted. For comparison, each satellite product was reprojected onto a $1^\circ \times 1^\circ$ grid for the African continent, as dictated by the resolution of the model forcing data, by averaging within each grid box all georeferenced, cloud free pixels, where the respective quality flags were of the highest rank.

[19] This intercomparison experiment was carried out for two different parameterizations of the model. First, a standard parameterization (denoted as model A), where soil parameters are derived from the global vegetation and soils data set of *Wilson and Henderson-Sellers* [1985]. Second, a modified parameterization (denoted as model B), where soil parameters are derived from the International Satellite Land Surface Climatology Project (ISLSCP) II soil data set [*Global Soil Data Task Group*, 2000]; with soil albedo from the data set of *Houldcroft et al.* [2009]. The assimilation experiment involved SEVIRI observations being assimilated into the most appropriate parameterization of JULES for a full year. This choice of EO product was made based on the correspondingly fine temporal resolution of both model and satellite product.

2.4. Remote Sensing Data

[20] SEVIRI acquires an image every 15 min, at a spatial resolution of between 3 km and 5 km for the African continent, and is the main payload on board the Meteosat Second Generation (MSG) geostationary satellites centered over the equator. A split-window algorithm for channels IR10.8 and IR12.0 is used to process LST data at an accuracy of 1.5 K [*Sobrino and Romaguera*, 2004] for most simulations between nadir and 50° viewing zenith angle. LST retrieval requires identification of cloudy/part cloudy pixels since clouds scatter and absorb IR radiance. The

Satellite Application Facility on Land Surface Analysis (LandSAF), whom generate and disseminate SEVIRI data, identify clear sky pixels through the application of a cloud mask which makes use of software developed by the Nowcasting and Very Short-Range Forecasting Satellite Application (NWC SAF; <https://www.nwcsaf.org>). This information is delivered in quality flags; and for this study, only pixels identified as cloud-free were used. A complete description of the LandSAF algorithm for LST retrievals can be found in the product user manual (available at the LandSAF web site <http://landsaf.meteo.pt/>).

[21] In this study, we used version 4 of the global MODIS LST product MOD11A1, which is acquired from thermal IR sensors on board the Sun-synchronous, near-polar-orbiting satellite Terra at a spatial resolution of 1 km. LST data is processed using a generalized split-window algorithm for bands 31 and 32 at a nominal accuracy better than 1.0 K [*Wan et al.*, 2004; *Wan*, 2008]. The large swath width of 2330 km allows data to be acquired for the African continent twice daily. A limitation of MODIS LST data is cloud contamination. MODIS LST data is accompanied by quality control flags; to minimize cloud contamination only pixels with the highest quality control flags were used.

[22] The swath width of the AATSR sensor on board the Sun-synchronous, polar-orbiting satellite Envisat is 512 km, with global coverage every 3 days and a repeat orbit of 35 days. Furthermore, measurements are available at two viewing angles, forward and nadir. For the purpose of LST studies however, only measurements from the nadir view, data set ATS_NR_2P, with a spatial resolution of 1 km are available. The uncertainty reported by *Coll et al.* [2005] for AATSR observations at nadir can be less than 1.0 K, depending on the algorithm and location; cloud contamination, though, is a limitation. Cloud identification is performed by the AATSR processor which identifies cloud affected pixels by applying a series of tests to the brightness temperature. If any test indicates the presence of clouds then this information is stored in the accompanying confidence flags. Full details of the LST retrieval algorithm can be found in the product user manual (available at the Envisat web site <http://envisat.esa.int/>).

2.5. LST Intercomparison

[23] For the intercomparison exercise observations over Africa were grouped as “day” (approximately 0700–1200 UTC); and “night” (approximately 1900–2400 UTC) to correspond with the Terra MODIS orbital overpass times. Variability of LST over brief temporal periods ensures validation of LST products is a challenging undertaking [*Pinheiro et al.*, 2006]. As stated in section 2.3, to account for the spatial variability satellite images were resampled to a $1^\circ \times 1^\circ$ grid to correspond with the JULES output. As for the temporal variability in the different sources, intercomparison between the modeled values and the satellite products was performed at individual 1° grid boxes only at a JULES time step when this corresponded both with a MODIS overpass time and with an AATSR overpass time, specifically when both these satellite images were classified as cloud-free, within a ± 10 min time window; and when the closest 15 min SEVIRI retrieval also resulted in cloud-free images. The monthly composites for the entire continent are an aggregation of all the individual grid box comparisons

carried out over the course of the month. First, the standard soil parameterization of JULES (model A) was run for each of the months of March, June, September, and December 2006 and compared with each of the EO products. Finally, this experiment was repeated under the modified soil parameterization (model B).

2.6. Data Assimilation

[24] Assimilation was carried out with the EnKF, which uses a Monte Carlo approach, and is a variant of the Kalman filter sequential assimilation method. The EnKF, first proposed by Evensen [1994], propagates an ensemble of states from which the state error covariance matrix can be determined from the distribution of the ensemble spread. The expensive integration of the state error covariance matrix is therefore avoided. In our data assimilation scheme, only LST is directly manipulated, where the state vector \mathbf{X}_{t+1} representing LST in all 2548 independent grid boxes at time $t + 1$ is defined as

$$\mathbf{X}_{t+1} = F(\mathbf{X}_t, \alpha_{t+1}, \beta) \quad (7)$$

where F is the model operator which in this case is JULES, and which operates on the state variable at time t , the meteorological forcing data (air temperature, downward long wave radiation, downward short wave radiation, precipitation, specific humidity, and surface pressure) at $t + 1$ represented by α_{t+1} , and the time-invariant model parameters represented by β .

[25] Starting from time $t = 0$, which is the initial state following model spin-up, each ensemble member of the forecast state vector \mathbf{X}_{t+1}^f at time $t + 1$ is propagated by adding stochastic forcing γ to equation (7) and is expressed as

$$\mathbf{X}_{t+1}^f = F(\mathbf{X}_t^a, \alpha_{t+1}, \beta) + \gamma \quad \gamma \sim N(0, \mathbf{P}) \quad (8)$$

where \mathbf{X}_t^a is the analysis state vector at time t . γ conforms to a Gaussian distribution with mean of zero and model error covariance \mathbf{P} . In the case of the initial condition of the assimilation run ($t = 0$), each ensemble member of the state vector \mathbf{X}_0^a is derived by adding random noise based on our knowledge of the model error which conforms to a Gaussian distribution with mean of zero and error covariance \mathbf{P}_0 . The model error strongly influences data assimilation performance; here model error was based on the standard deviation of the bias between the model simulations and in situ observations taken from a prior field campaign to the site of the Skukuza Eddy Covariance Tower in the Kruger National Park, South Africa, during July and August 2009. From this field data the mean model error was defined as 3.6 K. When observations for a grid box become available each ensemble member of the forecast state for that grid box is then updated by applying the update equation defined by Evensen [2003]:

$$\mathbf{X}^a = \mathbf{X}^f + \mathbf{K}(\mathbf{y} - \mathbf{H}\mathbf{X}^f + \varepsilon) \quad \varepsilon \sim N(0, \mathbf{R}) \quad (9)$$

where \mathbf{K} is the Kalman gain matrix, which determines the correction to the forecast state \mathbf{X}^f of the grid box, and is a function of the model error covariance matrix \mathbf{P} , and observation error covariance matrix \mathbf{R} :

$$\mathbf{K} = \mathbf{P}^f \mathbf{H}^T [\mathbf{H} \mathbf{P}^f \mathbf{H}^T + \mathbf{R}]^{-1} \quad (10)$$

[26] \mathbf{H} in equations (9) and (10) is the observation operator, which relates the model state variables to the observations. The observation \mathbf{y} is perturbed with stochastic forcing ε conforming to a Gaussian distribution with mean of zero and model error covariance \mathbf{R} . For the LST observations, the product uncertainty for SEVIRI measurements is used to determine its error range. In this case, the product uncertainty is defined as 1.5 K [Sobrino and Romaguera, 2004], which is comparable to the observation error of 1.6 K recorded during the field campaign to the site of the Skukuza Eddy Covariance Tower during July and August 2009.

[27] Equation (10) is traditionally solved by eigenvalue decomposition, whereby the cost of decomposition is a function of the ensemble size. The optimum number of ensemble members should therefore be determined for applying this method with minimal computational cost. The optimum estimate of the model state can be taken as the mean of the ensemble members [Burgers *et al.*, 1998; Evensen, 2003], with the variance around the mean a reflection of the uncertainty. As indicated in equations (2)–(5), LST (T_s) is a key variable for determining heat and water fluxes. The manipulations to LST carried out within our data assimilation scheme are propagated throughout the model structure affecting sensible and latent heat fluxes, and soil moisture.

[28] Assimilation was carried out using JULES (model B) over the duration of 2007. The resultant LST root-mean-square errors (RMSEs) were compared against the MODIS LST data set, since this can provide a context for an evaluation of the JULES model. Additionally, modeled estimates of surface soil moisture produced by JULES, with and without the assimilation of LST data, were compared with a surface soil moisture (SSM) data set derived at the Institute of Photogrammetry and Remote Sensing at the Vienna University of Technology, from radar backscattering coefficients produced from the active C-band (5.6 GHz) microwave scatterometer instruments on board the European Remote Sensing Satellites (ERS-1 and ERS-2). In our study, comparison between the model and the SSM data set was performed over an area of West Africa (15°W to 10°E longitude, 5°N to 20°N latitude) from 1 January to 31 May 2007. The SSM “observations” are generated from two separate ERS receiving stations (Maspalomas and Matera) covering this region of Africa.

[29] A detailed description of the change detection method for SSM retrieval is given by Wagner *et al.* [1999], but briefly, scatterometer estimates are used to model the incidence angle dependency of the radar backscattering coefficients, which are normalized to a 40° reference incidence angle. The relative SSM data, which ranges from 0% to 100%, are derived from the normalized coefficients, which are scaled between the driest and wettest observations over the long term. Validation studies of the ERS scatterometer SSM data set have been undertaken by Wagner *et al.* [1999], who compared the data set with gravimetric soil moisture measurements over Ukrainian field sites; and by Ceballos *et al.* [2005], who compared the data set with soil moisture from a network of 20 stations in western Spain. These studies recorded mean correlations of 0.41 and 0.75 in the top 100 cm soil profile. Furthermore, in their study, Ceballos *et al.* [2005] recorded a RMSE of 2.2%

between the scatterometer data and the average soil moisture. Additionally, it has been shown there is good agreement between the SSM data set and other soil moisture data sets in temperate, tropical and dry climates [Crow and Zhan, 2007; Pellarin et al., 2006; Wagner et al., 2003].

[30] In situ validation of the results was performed by analyzing the RMSEs of sensible (H) and latent heat (LE) fluxes, from both open loop modeling and following assimilation of LST, when compared with Eddy Covariance measurements [Papale et al., 2006]. These in situ measurements were obtained for a 3 month period, October–December 2007, from four African sites: the Skukuza flux tower (25.02°S, 31.50°E) in South Africa, situated in semi-arid savanna; the Mongu flux tower (15.44°S, 23.25°E) in Zambia, located in Miombo woodland; the Tchizalamou flux tower (4.29°S, 11.66°E) in the Congo, within a tropical savanna; and the Demokeya flux tower (13.28°N, 30.48°E) situated in a savanna/grassland area of the Sudan.

3. Results

3.1. LST Intercomparison

[31] Figure 1 shows both the SEVIRI daytime LST composite for the month of March 2006 and the difference between this nominal reference and both JULES (model A) and other satellite products. Since the composites are based on temporal retrievals when all four LST sources intersect within ± 10 min tolerance windows, the image gaps are a result of insufficient intersecting observations available to be able to construct a monthly composite. AATSR was found to be the remote sensing product with the highest mean temperatures, as well as displaying the largest standard deviation. MODIS was the product with the lowest mean temperatures, with the viewing angle generating noticeable effects (Figure 2); as the viewing angle increased the bias between SEVIRI and MODIS also increased. There is a general agreement between these findings and those of previous intercomparison studies. For instance, Trigo et al. [2008a] reported SEVIRI to systematically record higher surface temperatures than the MODIS product over Central Africa and the Iberian peninsula; and Noyes et al. [2006] found a similar tendency across ten sites in Europe and North Africa. This latter study also found AATSR to generate the highest mean LST of these products. The smaller range of view zenith angles for AATSR, compared with MODIS, means fewer pixels are affected by shadow and nondirect sunlight, resulting in a tendency to retrieve higher temperatures.

[32] Larger MODIS viewing angles were found to correspond with the largest daytime discrepancies in agreement with Trigo et al. [2008a]; a result one can reasonably assume to be a product of differential heating rates between sunlit and shadow scenes, whereas the SEVIRI geometry observes predominantly sunlit scenes. All three products displayed similar diurnal ranges, as reported in these two aforementioned studies. In the study of the Senegal River region by Stisen et al. [2007], however, the SEVIRI diurnal range was systematically larger than that of MODIS; a result that should warrant further investigation.

[33] LST simulated by model A is cooler than any of the satellite products (Table 1), with large negative biases occurring both during the day and the night. When each

IGBP land cover class was analyzed, it was found that the bias was most pronounced over barren or sparsely vegetated grid boxes. Results from the comparison during September produced the most striking differences between the modeled LST and the remote sensing products. One possible cause of this was an underestimation in the contribution of the bare soil tile LST to the grid box aggregate. Grid box LST in JULES is a linear combination of the associated tile LSTs and their corresponding fractional covers. However, in a two-source model surface temperature is defined as the fourth root of the aggregation of the fourth power of both soil and canopy LSTs multiplied by their corresponding fractional covers [Norman et al., 1995; Li et al., 2005]. Experimentation reveals only minimal improvement if the linear grid box averaging in JULES is substituted with this nonlinear approach; the largest adjustments being less than 0.1K, with these occurring in the savanna regions of the continent. Moreover, the barren or sparsely vegetated grid boxes consist almost exclusively of single tile components, whereby both aggregation methods produce the same LST.

[34] Although model representation of the average grid box LST could be a potential explanatory factor for a proportion of the bias where multiple tile fractions exist within a grid box, it was instead suspected that the prime candidate for model underestimation with respect to the remotely sensed LST was most likely to be the parameterization of the soil conditions. In order to investigate this further an alternative parameterization was experimented with (model B). This encompassed the use of the $1^\circ \times 1^\circ$ gridded data set of soil characteristics produced by ISLSCP II project [Global Soil Data Task Group, 2000] from the IGBP Data and Information System soil data set; and the soil albedo data set produced by the University of Swansea [Houldcroft et al., 2009]. Warmer signatures were obtained over much of the continent during March 2006 (Figure 3a), and resulted in a reduction in the mean monthly “daytime” continental bias between modeled LST and SEVIRI, from -5.39 K to -5.05 K; with the reduction being -8.87 K to -4.48 K for barren or sparsely vegetated grid boxes. The corresponding reduction during the “night” was -5.45 to -3.62 over the continent; and -7.62 to -5.59 over barren or sparsely vegetated grid boxes. It is the combination of the soil characteristics, such as soil moisture content and soil albedo (Figure 3b), which are responsible for the reduced bias between modeled LST from model B and SEVIRI LST. This experiment was repeated for June, September, and December 2006 with consistent reductions in bias achieved (Table 2). In spite of these reductions a residual bias still existed between model B and the SEVIRI product. In an assimilation system, such as the EnKF, a residual bias between the model and the observations prevents a statistically optimal analysis [Dee and da Silva, 1998]. The bias correction methodology of Reichle and Koster [2004] was therefore employed, in which the cumulative distribution functions (CDF) of the model and SEVIRI data were equated (Figure 4). This is an appropriate method, since CDF matching reduces systematic biases between model and observations without attributing the biases to a source [Drusch et al., 2005]. Here, the scaled SEVIRI LST denoted by x' was given by the solution to equation (11):

$$\text{CDF}_m(x') = \text{CDF}_s(x) \quad (11)$$

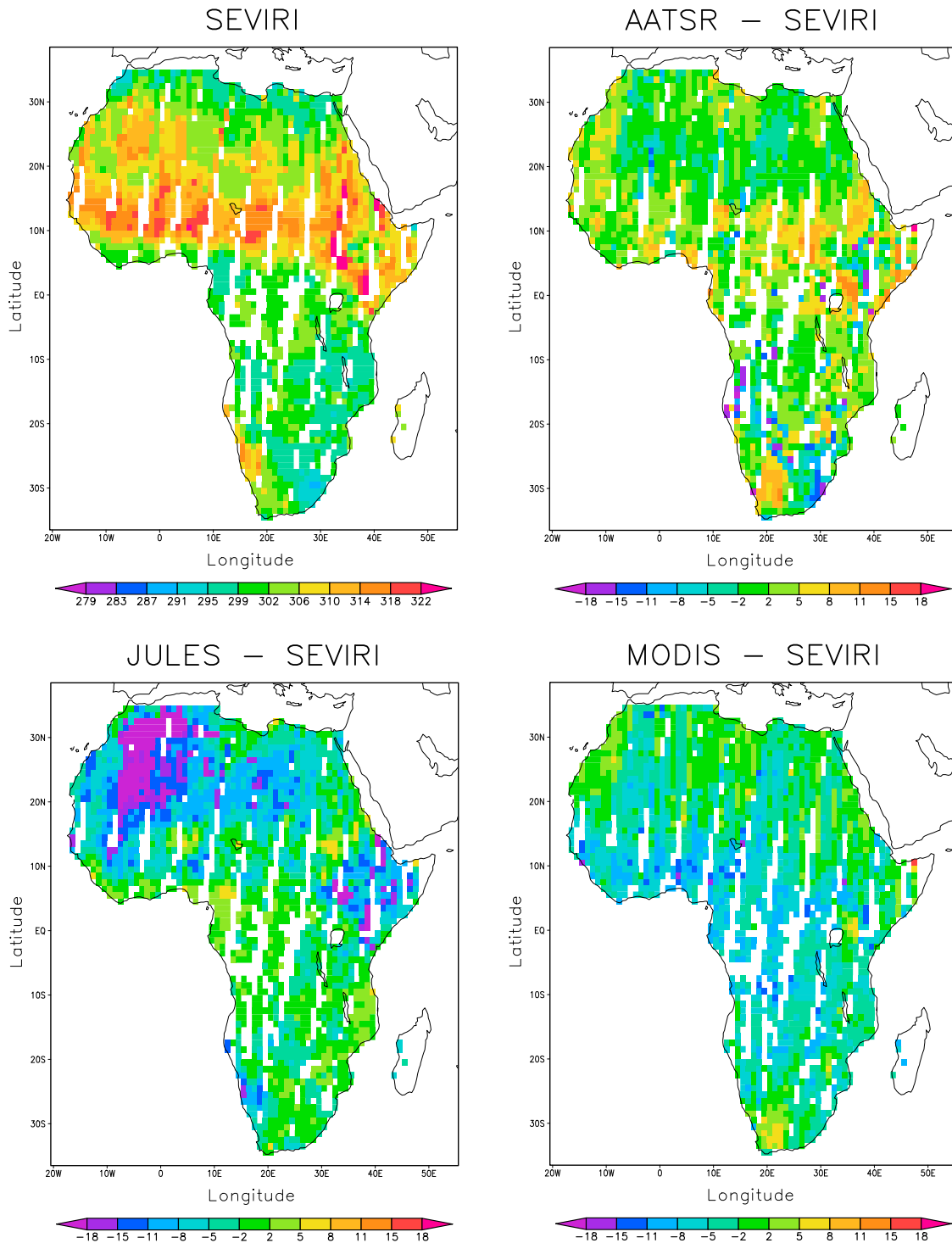


Figure 1. (top left) SEVIRI mean LST during March 2006 for day observations (approximately 0700–1200 UTC) displayed in absolute units and the difference between alternative LST sources and SEVIRI: (top right) AATSR minus SEVIRI, (bottom left) JULES model A minus SEVIRI, and (bottom right) MODIS minus SEVIRI. The monthly composites are based on temporal retrievals at JULES time steps whereby these coincided with both MODIS and AATSR overpass times within a ± 10 min tolerance, and the nearest 15 min SEVIRI retrieval was applied.

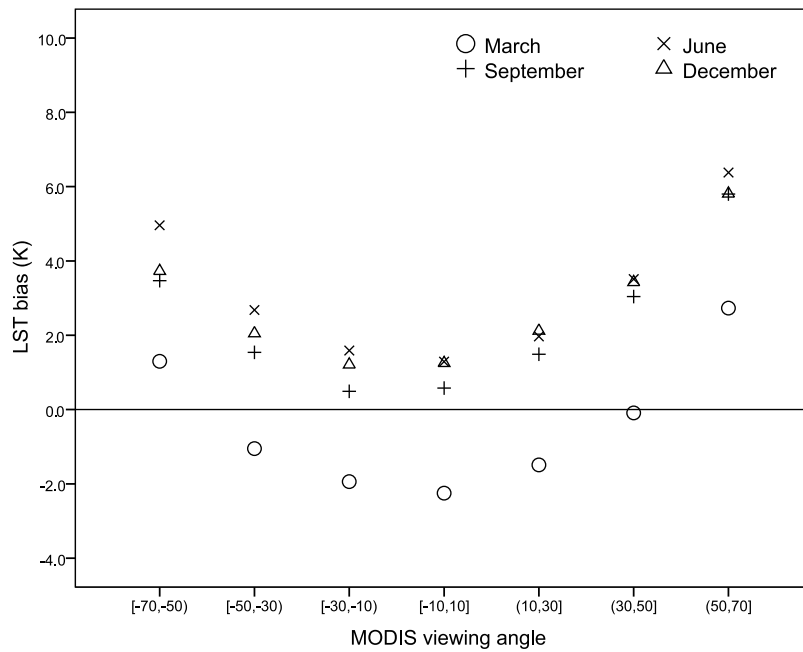


Figure 2. Bias between SEVIRI LST and MODIS LST for each of the 4 month assimilation periods in 2006 grouped by MODIS viewing angle.

where CDF_m and CDF_s denote the CDFs of the model LST and SEVIRI LST, respectively; with x being the unscaled SEVIRI LST.

3.2. Data Assimilation

[35] Following the bias correction, SEVIRI LST was assimilated into the model B parameterization of JULES for the entire year of 2007. An important step to undertake prior to assimilation analysis is to identify an optimum number of ensemble members. Figure 5 identifies a considerable reduction in RMSE, with respect to MODIS LST, when even a small ensemble size is used in comparison to the modeled scenario. This reduction continues as the number of ensemble members is increased, but at a decreasing rate. Since increased ensemble size corresponds to an increased

Table 1. Mean Day (Approximately 0700–1200 UTC) and Night (Approximately 1900–2400 UTC) Biases, Covering the 4 Month Comparison Periods of March, June, September, and December 2006, Between Modeled LST (Model A) and Remote Sensing Products for the Continental Landmass and for the Barren or Sparsely Vegetated IGBP Land Cover Class

Month	Continental Bias (K)			Barren or Sparsely Vegetated Bias (K)		
	AATSR	MODIS	SEVIRI	AATSR	MODIS	SEVIRI
<i>Day</i>						
March	-6.76	-1.85	-5.39	-9.40	-6.56	-8.87
June	-6.81	-2.14	-5.48	-11.74	-7.33	-10.33
September	-11.21	-5.27	-7.47	-17.62	-10.19	-12.06
December	-6.52	-2.25	-5.50	-6.87	-5.19	-8.08
<i>Night</i>						
March	-3.27	-0.12	-5.45	-3.92	-2.57	-7.62
June	-7.37	-2.20	-5.46	-9.96	-6.05	-9.18
September	-8.49	-4.33	-7.54	-11.52	-8.12	-11.23
December	-2.31	0.71	-1.15	-1.88	-0.71	-3.17

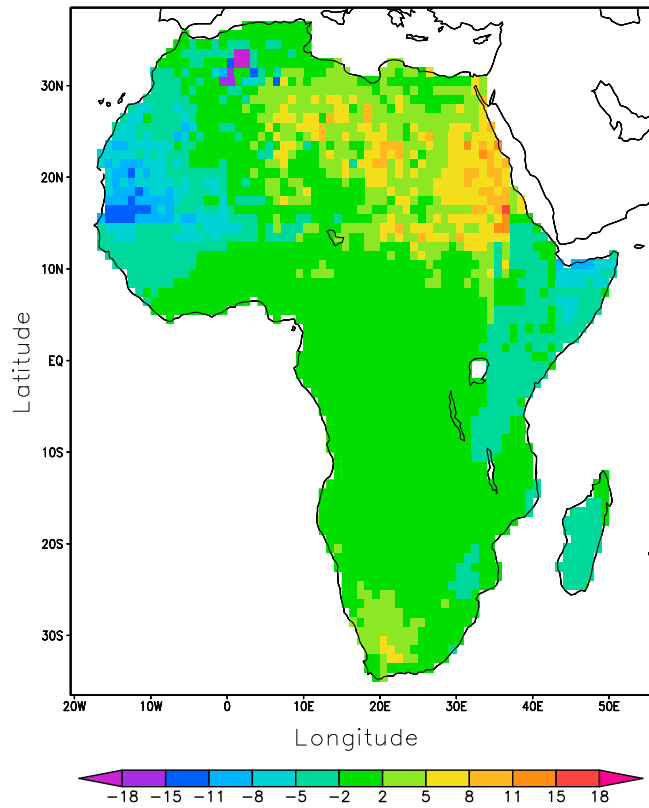


Figure 3a. Mean daytime (approximately 0700–1200 UTC) LST difference, during March 2006, between the JULES model with alternative thermal, hydrologic, and albedo soil parameters (model B) and the JULES model with standard soil parameters (model A).

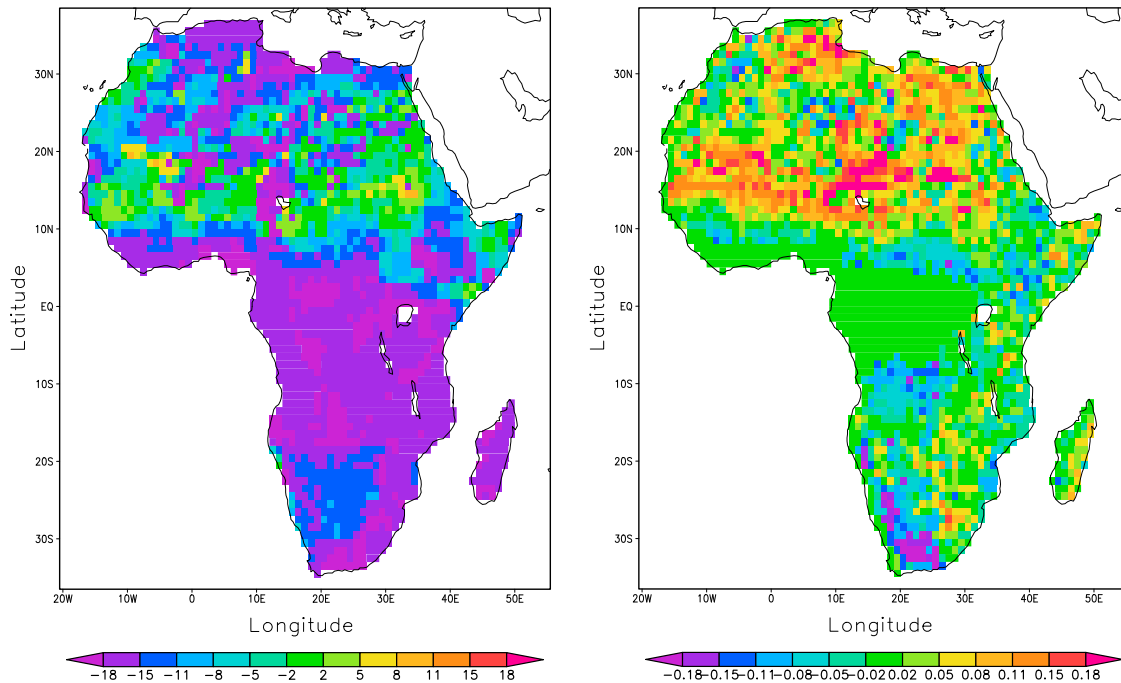


Figure 3b. Differences in selected soil characteristics between model B and model A during March 2006: (left) soil moisture content and (right) soil albedo.

computational burden, the desired number of ensemble members should maximize the RMSE reduction while minimizing the computational load. For the assimilation experiment an ensemble size of 100 was chosen, as any further reductions in RMSEs for larger ensemble sizes were minimal.

[36] The time series of LST for 2007 (Figure 6) illustrates the change in JULES LST in the context of the MODIS LST. What we found was that the model predictions under the influence of data assimilation were more comparable with this alternative LST data set than were the modeled values; with a 54.5% reduction in RMSE from 2.11 K to 0.96 K. Larger adjustments were experienced during the middle of the year, due to larger changes during the hottest hours of each day for this period of the year; whereas the start and end of the year experienced reductions in LST as a result of greater changes during the night but in a downward direction.

[37] Furthermore, a comparison was made between the soil moisture outputs of the model with and without LST data assimilation, and SSM scatterometer values in the top 5 cm of the soil over an area of West Africa for the first 5 months of 2007 (Figure 7). The modeled values are clearly higher than the SSM “observations” derived from the ERS scatterometer. Following assimilation, the updated model estimates are closer to the “observation” values. This can be quantified as a 21.6% reduction in RMSE, from 17.1vol% to 13.4vol% between the model estimates and the ERS scatterometer “observations.” A t statistic of 10.4, generated from t tests assuming equal variances on the mean RMSEs from 50 repeated open loop and model runs with LST data assimilation, indicated that these reductions in RMSE were significant at the 99% confidence level. The spatial distribution

of the differences between these updated model estimates following LST assimilation and the model estimates without data assimilation are illustrated in Figure 8. Corresponding time series for evapotranspiration (ET) and LE over the same geographical area for this 5 month period are illustrated in Figure 9; whereby the changes in LE are driven by changes in ET.

[38] During 2007, the values of H and LE fluxes for open loop and model runs with LST data assimilation were compared against in situ measurements from Skukuza, Mongu, Tchizalamou, and Demokeya from October to December (Table 3). This was the only period of sufficient collection from all of these sites during this year. Reductions in

Table 2. Mean Day (Approximately 0700–1200 UTC) and Night (Approximately 1900–2400 UTC) Biases, Covering the 4 Month Comparison Periods of March, June, September, and December 2006, Between Modeled LST (Model B) and Remote Sensing Products for the Continental Landmass and for the Barren or Sparsely Vegetated IGBP Land Cover Class

Month	Continental Bias (K)			Barren or Sparsely Vegetated Bias (K)		
	AATSR	MODIS	SEVIRI	AATSR	MODIS	SEVIRI
	<i>Day</i>					
March	-6.42	-1.51	-5.05	-5.01	-2.16	-4.48
June	-5.13	-0.45	-3.79	-5.82	-1.41	-4.41
September	-7.94	-2.00	-4.21	-10.78	-3.36	-5.23
December	-4.83	-0.55	-3.81	-2.52	-0.85	-3.74
	<i>Night</i>					
March	-1.44	1.71	-3.62	-1.89	-0.53	-5.59
June	-2.55	2.62	-0.64	-2.77	1.14	-1.99
September	-3.22	0.95	-2.27	-3.69	-0.28	-3.40
December	-2.11	0.91	-0.95	-1.59	-0.42	-2.88

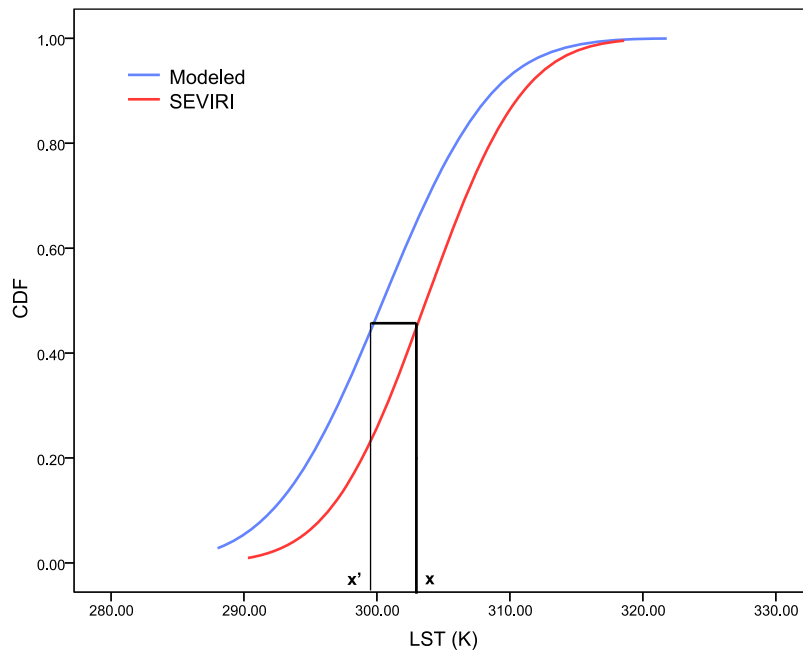


Figure 4. The average cumulative distribution function (CDF) of both the modeled LST and the SEVIRI LST. The bold arrows illustrate schematically how the unscaled SEVIRI observation x is converted into the scaled observation x' using CDF matching.

RMSE were recorded for both H and LE fluxes from the assimilation runs, compared with the respective fluxes from the standard model runs, with respect to the fluxes recorded at all four Eddy Covariance towers. The reduction in RMSE of H with respect to the flux recorded at Demokeya shows the strongest reduction of uncertainty through the LST data assimilation. When these reductions were tested on 50 repeated open loop and model runs with LST data assimilation using t

tests assuming equal variances, all the reductions were significant at the 95% confidence level, with six of these being significant at the 99% confidence level.

4. Discussion

[39] LST validation with ground measurements can be both time consuming, and limited in its geographical extent.

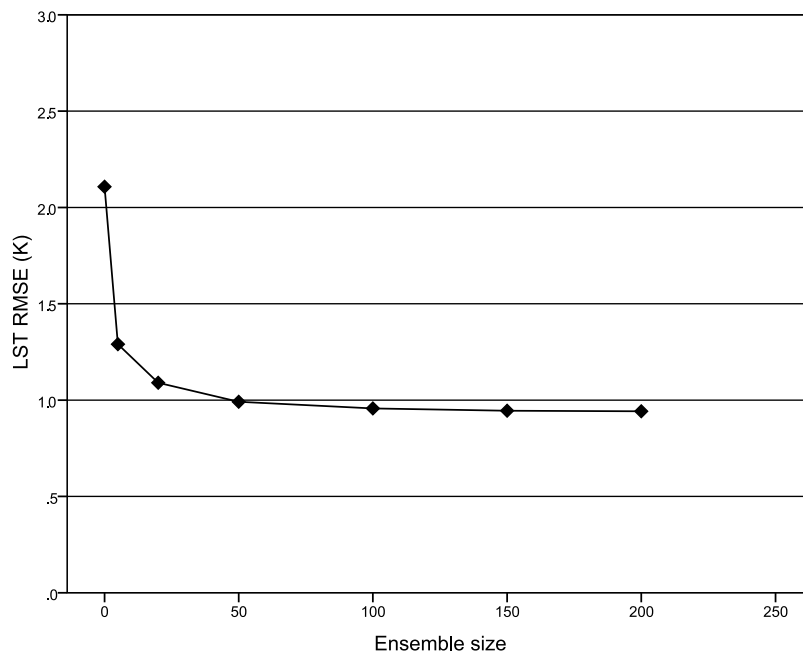


Figure 5. Comparison test of the results from the assimilation of SEVIRI LST into the JULES model for the entire year 2007, showing LST RMSEs with respect to MODIS LST observations for experiments with different ensemble sizes.

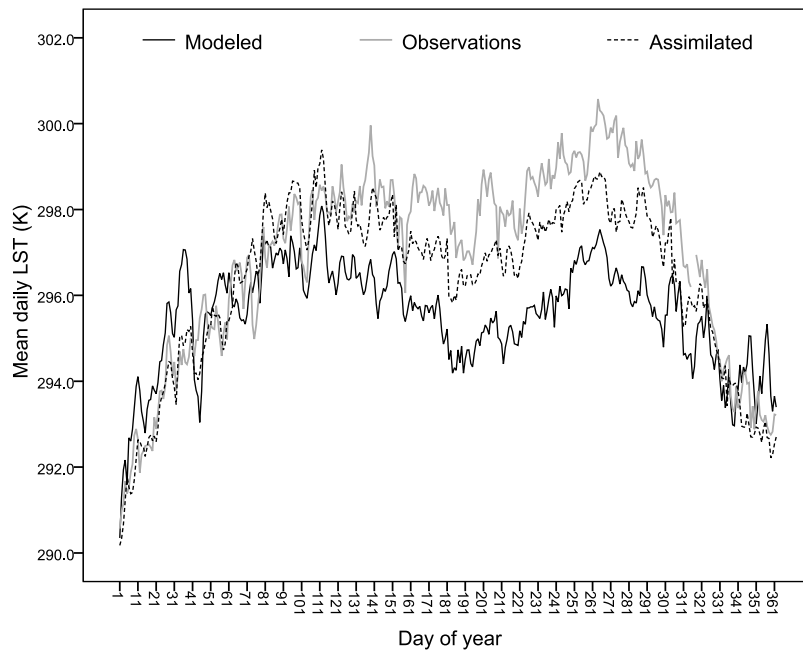


Figure 6. Time series of open loop modeling versus model run following assimilation of mean daily LST for the continental landmass covering the entire year 2007. MODIS observations are plotted for comparison.

An intercomparison exercise between thermal products generated aboard EO satellites provides a more realistic alternative over large spatial and temporal scales; with these products also representing the most feasible source of observation values for assimilating into regional and global parameterizations of land surface models, such as the UK Met Office’s JULES model. A caveat to the intercomparison

test carried out here is that due to cloud contamination, available MODIS LST products were limited. Indeed, cloud masking makes any intercomparison a more challenging undertaking, as fewer pixels are available for analysis. However, an improvement could be achieved with the use of the latest MODIS LST version (V5), which includes a refinement in the cloud screening process [Wan, 2008].

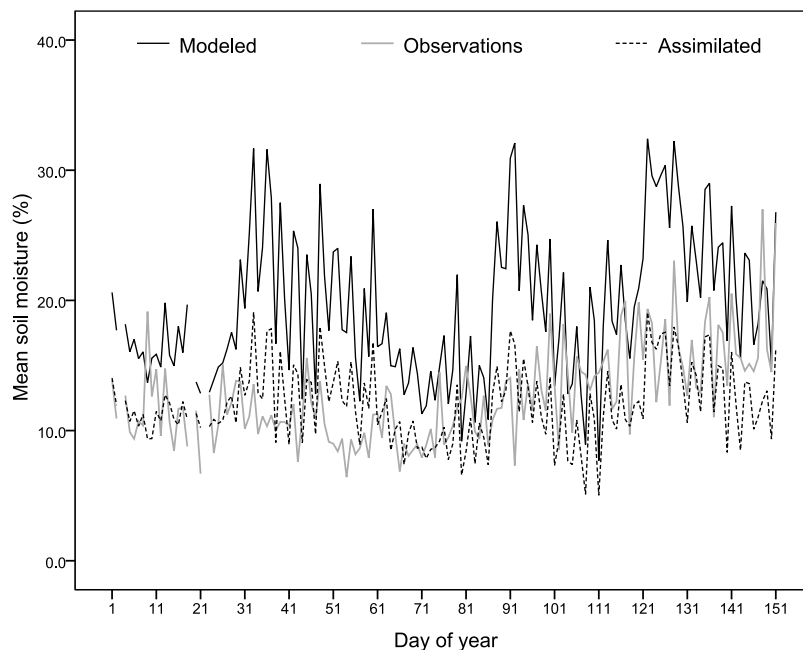


Figure 7. Time series of open loop modeling versus model run following LST assimilation for values over a region of West Africa (15°W to 10°E longitude, 5°N to 20°N latitude) from 1 January to 31 May 2007 of mean daily soil moisture in the top 5 cm of the soil profile. ERS scatterometer surface soil moisture observations from the top 5 cm of the soil profile are plotted for comparison.

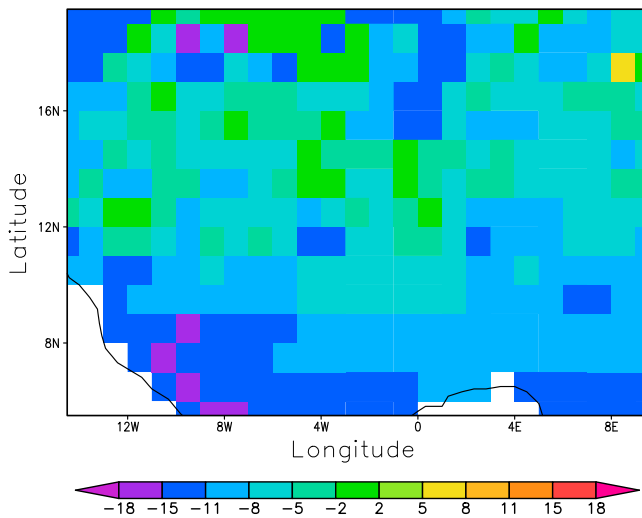


Figure 8. Mean daily soil moisture difference in the top 5 cm of the soil profile between the open loop model run and the model run following LST assimilation over a region of West Africa (15°W to 10°E longitude, 5°N to 20°N latitude) from 1 January to 31 May 2007.

Even so, the loss of pixels to cloud contamination is limiting, particularly for the comparison with AATSR retrievals due to the longer repeat cycle.

[40] JULES is an evolving land surface model, whereby recent studies [Alton *et al.*, 2007b; Mercado *et al.*, 2007] have made improvements to the standard implementation. Furthermore, recent sensitivity and validation analyses of JULES [Alton *et al.*, 2007a; de Rosnay *et al.*, 2009; Weber *et al.*, 2009] have established confidence in the biophysical representations of ecosystem processes in tropical biomes, including those covering Africa. Data assimilation represents the next logical step in further improving the reliability of the model and reducing uncertainties inherent in all such land surface models.

[41] A variable with potentially far-reaching influence in land surface models is LST. In JULES this variable is derived from the surface energy balance. When this was compared with the satellite-derived LST data, we found the model underestimated LST when compared with all three satellite-derived LST data sets during the entire diurnal cycle, with larger biases experienced for less vegetated surface types (Table 1). We suggest several possible explanations for this discrepancy. First, there is a tendency for satellite-derived LST data to systematically overestimate in situ measurements. This occurrence was reported by Trigo *et al.* [2008a] for SEVIRI observations, with possible explanations of sensor calibration and a favoring of sunlit surfaces being proposed. Second, the assumptions present in the algorithms for generating high-level thermal products may be inconsistent with those in the land surface model, resulting maybe in an inadequate processing of long wave emissivity in JULES, which has not been investigated here and will require further examination. Finally, the parameterization of thermal and hydrological soil characteristics do not appropriately represent the spatial heterogeneity of these qualities for sparsely vegetated regions. This is pertinent since the bare soil surface temperature in JULES is quantified from the temperature of the upper layer in the soil profile as well as the surface energy balance equation. This final possibility provided motivation for the study by Houldcroft *et al.* [2009] to improve the description of surface albedo in land surface models.

[42] When this modified soil albedo data set, derived from the MODIS MCD43C1 albedo product, was employed in the model, and the standard soil parameters from the global vegetation and soils data set of Wilson and Henderson-Sellers [1985] were substituted for parameters derived from the ISLSCP II soil data set, a reduction in the biases between model and EO products was recorded. It is reasonable to accept this improvement with the recognition that soil moisture, and surface albedo, are two of the most significant determining factors in LST variability [Goward *et al.*, 2002]. Soil moisture has a significant influence on

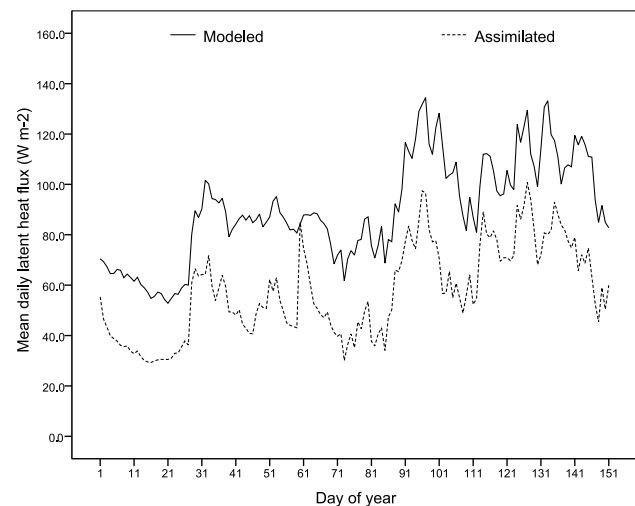
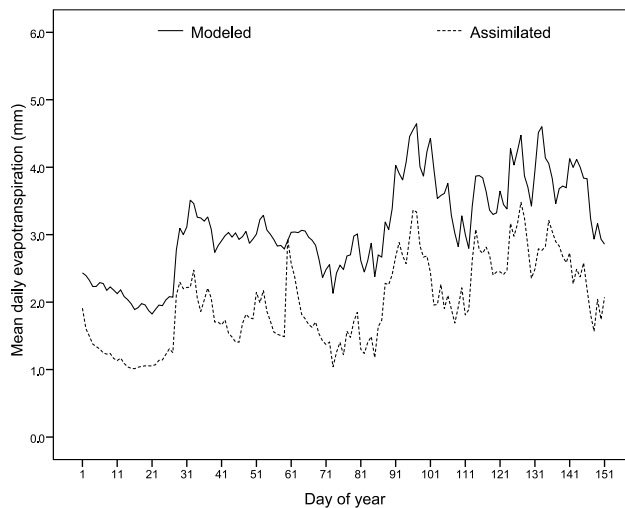


Figure 9. Time series of open loop modeling versus model run following LST assimilation for values over a region of West Africa (15°W to 10°E longitude, 5°N to 20°N latitude) from 1 January to 31 May 2007 of (left) mean daily evapotranspiration and (right) mean daily latent heat flux.

Table 3. Evaluation of Open Loop Modeling and Model Run Following LST Assimilation With Respect to 1-Hourly Eddy Covariance Measurements of Sensible and Latent Heat Fluxes From Four African Sites Covering the Period October–December 2007^a

	RMSE (W m ⁻²)		Reduction (%)	<i>t</i> Statistic ^b
	Modeled	Assimilated		
Skukuza				
H	30.76	28.66	6.83	5.066**
LE	47.52	43.17	9.15	10.935**
Mongu				
H	41.42	40.56	2.08	2.251*
LE	49.21	47.29	3.90	4.441**
Tchizalamou				
H	27.18	24.26	10.74	7.620**
LE	41.30	39.48	4.41	4.938**
Demokeya				
H	54.15	40.78	24.69	35.393**
LE	41.07	40.31	1.85	1.993*

^aAfrican sites: Skukuza, South Africa; Mongu, Zambia; Tchizalamou, Congo; and Demokeya, Sudan. The percentage reduction in RMSE is given along with the *t* statistic and an indication of significance of the one-tailed *t* test. The *t* tests assuming equal variances were performed on the mean RMSEs from 50 repeated runs of the model. H, sensible heat flux; LE, latent heat flux.

^b**, significance at the 0.99 level; *, significance at the 0.95 level.

the partitioning of energy into sensible and latent heat fluxes. For instance, a wet soil surface is cooler and loses more latent heat, whereas a dry soil surface generally corresponds to higher surface temperatures and loses more sensible heat [Smith *et al.*, 2006]. Surface albedo, determines the amount of energy absorbed by the land surface. The modified albedo data set developed for land surface modeling is more comparable with EO albedo products, particularly over sparsely vegetated regions [Houldcroft *et al.*, 2009].

[43] Probably all land surface models, including JULES, are limited by the accuracy to which their representation of physical processes imitate the terrestrial biosphere. Optimization of variable estimation, such as LST, can be achieved by assimilating observation data into the model through a mechanism like the EnKF. This technique balances the uncertainty in both the model and observations, but is subject to sampling errors which are a function of the ensemble size [Evensen, 2003]. It is therefore important to select an appropriately sized ensemble that on the one hand minimizes the sampling errors and obtains satisfactory results, whereas concurrently reducing the computational burden.

[44] Moreover, EnKF data assimilation over land is often based on covariance localization methods, in which sampled cross covariances between geographically disparate points are explicitly set to zero. The concept here is to subdivide the global analysis into smaller subdomains which are independently analyzed based only on local observations, with these subdomains simultaneously updated in parallel as implemented by Hamill *et al.* [2001] and Houtekamer and Mitchell [2001]. This requirement is because of the uncertainties in sampling cross covariances using finite ensemble sizes, and the possibility of creating spurious cross correlations. Indeed, Reichle and Koster [2003] have found covariance localization to increase the accuracy of estimations for small ensemble sizes in particular. In this study analysis is subdivided into the individual model grid cells

which are independent of each other since no lateral fluxes exist in JULES.

[45] The reduction in RMSE with respect to MODIS LST is clearly discernable as the ensemble size is initially increased, with further improvement experienced at a decreasing rate for larger ensemble sizes (Figure 5). Indeed when *t* tests assuming equal variances were performed on the mean RMSEs from 50 repeated runs, the reduction in RMSE remained statistically significant at the 5% level even when the ensemble size was increased from 50 to 100, but this ceased to be the case when the ensemble size was further increased to 150. The chosen size of 100 therefore produced acceptable results, whereby a further increase in size to 150 did not significantly improve the EnKF results.

[46] Much of the shift in the LST as a result of assimilation occurred during the hottest parts of each day, particularly for regions with sparse vegetation coverage. One possibility for this occurrence could be that the model is simulating suboptimal diffusion of heat between the land surface and the topsoil layer, thereby producing large variances in the LST estimations. A caveat to these findings is that although the observation perturbations remain constrained by a fixed product uncertainty; the lower dependency on the differential heating or cooling of the surface, a result of sunlit or shadow areas, during the daytime could result in observation errors that are larger than the applied product uncertainty. Indeed, SEVIRI observations during the daytime hours are reported to regularly fail to meet the accuracy target of the satellite application facility on land surface analysis (LandSAF), who generate and disseminate SEVIRI data, of 2.0 K over desert and semiarid regions [Trigo *et al.*, 2008b].

[47] It is evident from Figure 7 that a reduction in the model predictions of soil moisture over an area of West Africa for the period 1 January to 31 May 2007 has resulted through the process of data assimilation. This corresponds to reductions in both ET and LE experienced for this same spatial and temporal window (Figure 9). The ET rate is controlled by stomatal conductance, which is affected by the quantity of photosynthetically active radiation. Furthermore, the positive relationship between ET and net primary productivity (NPP), as suggested by Rosenzweig [1968], implies the assimilation of LST also has the potential to influence the interannual variability in the carbon cycle.

[48] Additionally, the change in LST influences the H flux, whereby the increase in surface energy is differentially partitioned into H and LE, as a result of the changes in the temperature and humidity gradients in the surface boundary layer, respectively. This is a consequence of the proportional changes to LST experienced over the vegetated and nonvegetated fractions of each grid box. The result of these changes in the surface energy budget is that reductions in RMSEs for H and LE fluxes are observed when evaluated against in situ measurements (Table 3). Although the magnitude of the RMSE reductions when compared with measurements taken during the final 3 months of 2007 from Skukuza, Mongu and Tchizalamou are relatively small, a possible reason may be because of the higher vegetative cover during the southern African wet season; whereas a larger RMSE reduction was experienced for sensible heat flux when compared for the Demokeya site. This site is located in more sparsely vegetated ground, and is subject to

the lowest annual precipitation (320 mm) of the four sites; in comparison to Tchizalamou (1150 mm), Mongu (945 mm) and Skukuza (547 mm). Moreover, the final 3 months of 2007 correspond to the beginning of the dry season at Demokeya. Indeed, it is likely large RMSE reductions could also be experienced at alternative sites located within sparsely vegetated ground. Further investigation is thus required of the JULES model to see if LE and H are accurately simulated at other African ground stations across a range of biomes.

[49] It is feasible that changes to a key variable, such as LST, could have a detrimental impact upon the energy fluxes within the model. Despite the fact that reductions in RMSEs for H and LE fluxes were relatively small, with respect to the eddy covariance measurements, the changes to these fluxes did not result in any increase in RMSE. Overall, when considering these findings, it can be argued that a benefit could be gained in updating the modeled state with remotely sensed observations using an EnKF. This would be consistent with findings from previous studies, such as those by Huang *et al.* [2008] and Pipunic *et al.* [2008].

[50] Although promising in nature, these findings are based upon updating model LST by assimilating frequent observations from the SEVIRI sensor onboard the geostationary MSG satellites. The temporal memory of JULES LST is limited to the previous 30 or 60 min time step. This may not be significant when the observations are the frequent SEVIRI retrievals, but can become pertinent for less frequent remote sensing observations from polar-orbiting satellites. Future research, utilizing an alternative observation operator, could therefore examine updating variables in JULES with longer memory, such as soil temperature, through the assimilation of remotely sensed LST products with less frequent retrievals, such as MODIS or AATSR.

5. Conclusions

[51] This paper has considered the importance of LST as an integral component in the calculation of surface to atmosphere heat fluxes, and has investigated a technique to constrain the estimations within a state-of-the-art land surface model. An intercomparison was carried out between the model simulated LST and various thermal remote sensing products. This represented an attractive alternative to verification with in situ measurements, which are sparsely located and may not easily represent a heterogeneous grid box. Satellite-derived LST estimates were then assimilated into the land surface model using an EnKF filter.

[52] Although differences exist for sparsely vegetated regions, LST simulated by JULES is comparable with remotely sensed LST products. In light of the sensitivity of the LST to changes in soil albedo and soil thermal and hydrologic characteristics however, further investigation into the soil parameterization of JULES merits attention. The differences between the model and satellite observations of LST can additionally be reduced through data assimilation. Our results indicate that data assimilation can indeed prove to be a consistent and reliable method of constraining the simulations of complex biophysical land surface models. Despite the ensemble size being one of the most sensitive approximations in the EnKF formulation, we

found that satisfactory improvements can be made with relatively few ensemble members.

[53] This study represents the first step in producing an operational data assimilation scheme for the JULES model; and indeed further work is also required in optimizing soil parameters, particularly where LSTs are considerably underestimated, with vegetation parameterization also worthy of closer investigation. Following these promising results in the experiments of LST assimilation, further work can be carried out both in the assimilation of LST from less temporally frequent sources, such as MODIS and AATSR; and remotely sensed vegetation indices, such as NDVI data, thereby constraining the estimation of a surface dryness index to estimate live FMC; an important variable in modeling fire occurrence and propagation. Indeed, data assimilation offers the opportunity of integrating numerous reflectance products into land surface models with the prospect of reducing the considerable uncertainties in the simulation of biogeochemical fluxes.

[54] **Acknowledgments.** This work has been funded by the NERC Climate and Land Surface Systems Interactions Centre (CLASSIC). The work was also supported by the CARBOAFRICA project, funded by the EU Framework Programme 6, proposal 037132. The authors would like to thank Stefan Hasenauer at the Institute of Photogrammetry and Remote Sensing, Vienna University of Technology, for providing the ERS scatterometer surface soil moisture data set and for advice on its use. We would also like to acknowledge Phil Harris at the Centre for Ecology and Hydrology, Wallingford, United Kingdom, for the provision of the soil albedo data file and Bob Scholes and his team at CSIR Natural Resources and the Environment, Pretoria, South Africa, for providing the in situ measurements from the Skukuza Flux Tower. Finally, we would like to thank Elizabeth Noyes at the UK Met Office, Exeter, for the valuable input pertaining to the data retrieval and processing from the AATSR and SEVIRI EO sensors.

References

- Alton, P., L. Mercado, and P. North (2007a), A sensitivity analysis of the land-surface scheme JULES conducted for three forest biomes: Biophysical processes, model processes, and meteorological driving data, *Global Biogeochem. Cycles*, *20*, GB1008, doi:10.1029/2005GB002653.
- Alton, P. B., P. R. North, and S. O. Los (2007b), The impact of diffuse sunlight on canopy light-use efficiency, gross photosynthetic product and net ecosystem exchange in three forest biomes, *Global Change Biol.*, *13*(4), 776–787.
- Bosilovich, M. G., J. D. Radakovich, A. da Silva, R. Todling, and F. Verter (2007), Skin temperature analysis and bias correction in a coupled land-atmosphere data assimilation system, *J. Meteorol. Soc. Jpn.*, *85A*, 205–228, doi:10.2151/jmsj.85A.205.
- Burgers, G., P. J. van Leeuwen, and G. Evensen (1998), Analysis scheme in the ensemble Kalman filter, *Mon. Weather Rev.*, *126*(6), 1719–1724, doi:10.1175/1520-0493(1998)126<1719:ASITEK>2.0.CO;2.
- Byrne, G. F., J. E. Begg, P. M. Fleming, and F. X. Dunin (1979), Remotely sensed land cover temperature and soil-water status: Brief review, *Remote Sens. Environ.*, *8*(4), 291–305, doi:10.1016/0034-4257(79)90029-4.
- Ceballos, A., K. Scipal, W. Wagner, and J. Martinez-Fernandez (2005), Validation and downscaling of ERS scatterometer derived soil moisture data over the central part of the Duero Basin, Spain, *Hydrol. Processes*, *19*, 1549–1566, doi:10.1002/hyp.5585.
- Coll, C., V. Caselles, J. M. Galve, E. Valor, R. Niclos, J. M. Sanchez, and R. Rivas (2005), Ground measurements for the validation of land surface temperatures derived from AATSR and MODIS data, *Remote Sens. Environ.*, *97*(3), 288–300, doi:10.1016/j.rse.2005.05.007.
- Cox, P. M., R. A. Betts, C. B. Bunton, R. L. H. Essery, P. R. Rowntree, and J. Smith (1999), The impact of new land surface physics on the GCM simulation of climate and climate sensitivity, *Clim. Dyn.*, *15*(3), 183–203, doi:10.1007/s003820050276.
- Crow, W. T., and X. Zhan (2007), Continental-scale evaluation of remotely sensed soil moisture products, *IEEE Geosci. Remote Sens. Lett.*, *4*, 451–455, doi:10.1109/LGRS.2007.896533.

- Dee, D. P., and A. da Silva (1998), Data assimilation in the presence of forecast bias, *Q. J. R. Meteorol. Soc.*, 124(545), 269–295, doi:10.1002/qj.49712454512.
- de Rosnay, P., et al. (2009), AMMA Land Surface Model Intercomparison Experiment coupled to the Community Microwave Emission Model: ALMIP-MEM, *J. Geophys. Res.*, 114, D05108, doi:10.1029/2008JD010724.
- Drusch, M., E. F. Wood, and H. Gao (2005), Observation operators for the direct assimilation of TRMM microwave imager retrieved soil moisture, *J. Geophys. Res. Lett.*, 32, L15403, doi:10.1029/2005GL023623.
- Dunderdale, M., J. P. Muller, and P. M. Cox (1999), Sensitivity of the Hadley Centre climate model to different earth observation and cartographically derived land surface data-sets, in *Proceedings of ALPS99 Workshop: Ocean Color, Land Surfaces, Radiation and Clouds, Aerosols: The Contribution of POLDER and New Generation Spaceborne Sensors to Global Change Studies*, pp. 1–6, Cent. Nat. d'Etudes Spatiales, Meribel, France.
- Evensen, G. (1994), Sequential data assimilation with a nonlinear quasi-geostrophic model using Monte Carlo methods to forecast error statistics, *J. Geophys. Res.*, 99(C5), 10,143–10,162, doi:10.1029/94JC00572.
- Evensen, G. (2003), The ensemble Kalman filter: Theoretical formulation and practical implementation, *Ocean Dyn.*, 53, 343–367, doi:10.1007/s10236-003-0036-9.
- Ge, J., J. Qi, and B. Lofgren (2008), Use of vegetation properties from EOS observations for land-climate modeling in East Africa, *J. Geophys. Res.*, 113(D15), D15101, doi:10.1029/2007JD009628.
- Gelb, A. (1974), *Applied Optimal Estimation*, 374 pp., MIT Press, Cambridge, Mass.
- Global Soil Data Task Group (2000), Global Gridded Surfaces of Selected Soil Characteristics (IGBP-DIS), International Geosphere-Biosphere Programme, Data and Information System, <http://www.daac.ornl.gov/>, Distrib. Active Arch. Cent., Oak Ridge Natl. Lab., Oak Ridge, Tenn.
- Goward, S. N., Y. Xue, and K. P. Czajkowski (2002), Evaluating land surface moisture conditions from the remotely sensed temperature/vegetation index measurements: An exploration with the simplified simple biosphere model, *Remote Sens. Environ.*, 79(2–3), 225–242, doi:10.1016/S0034-4257(01)00275-9.
- Hamill, T. M., J. S. Whitaker, and C. Snyder (2001), Distance-dependent filtering of background error covariance estimates in an ensemble Kalman filter, *Mon. Weather Rev.*, 129(11), 2776–2790, doi:10.1175/1520-0493(2001)129<2776:DDFOBE>2.0.CO;2.
- Hashimoto, H., J. L. Dungan, M. A. White, F. Yang, A. R. Michaelis, S. W. Running, and R. R. Nemani (2008), Satellite-based estimation of surface vapor pressure deficits using MODIS land surface temperature data, *Remote Sens. Environ.*, 112(1), 142–155, doi:10.1016/j.rse.2007.04.016.
- Houldcroft, C. J., W. M. F. Grey, M. Barnsley, C. M. Taylor, S. O. Los, and P. R. J. North (2009), New vegetation albedo parameters and global fields of soil background albedo derived from MODIS for use in a climate model, *J. Hydrometeorol.*, 10(1), 183–198, doi:10.1175/2008JHM1021.1.
- Houtekamer, P. L., and H. L. Mitchell (2001), A sequential ensemble Kalman filter for atmospheric data assimilation, *Mon. Weather Rev.*, 129(1), 123–137, doi:10.1175/1520-0493(2001)129<0123:ASEKFF>2.0.CO;2.
- Huang, C. L., X. Li, and L. Lu (2008), Retrieving soil temperature profile by assimilating MODIS LST products with ensemble Kalman filter, *Remote Sens. Environ.*, 112(4), 1320–1336, doi:10.1016/j.rse.2007.03.028.
- Hughes, J. K., P. J. Valdes, and R. Betts (2006), Dynamics of a global-scale vegetation model, *Ecol. Modell.*, 198(3–4), 452–462, doi:10.1016/j.ecolmodel.2006.05.020.
- Hulme, M., R. Doherty, T. Ngara, M. New, and D. Lister (2001), African climate change: 1900–2100, *Clim. Res.*, 17(2), 145–168, doi:10.3354/cr017145.
- Ichii, K., H. Hashimoto, R. Nemani, and M. White (2005), Modeling the interannual variability and trends in gross and net primary productivity of tropical forests from 1982 to 1999, *Global Planet. Change*, 48(4), 274–286, doi:10.1016/j.gloplacha.2005.02.005.
- Intergovernmental Panel on Climate Change (IPCC) (2007), *Climate Change 2007: The Physical Science Basis: Working Group I Contribution to the Fourth Assessment Report of the IPCC*, edited by S. Solomon et al., Cambridge Univ. Press, New York.
- Jin, M., R. E. Dickinson, and A. M. Vogelmann (1997), A comparison of CCM2-BATS skin temperature and surface-air temperature with satellite and surface observations, *J. Clim.*, 10(7), 1505–1524, doi:10.1175/1520-0442(1997)010<1505:ACOCBS>2.0.CO;2.
- Kalnay, E., et al. (1996), The NCEP/NCAR 40-year reanalysis project, *Bull. Am. Meteorol. Soc.*, 77(3), 437–471, doi:10.1175/1520-0477(1996)077<0437:TNYRP>2.0.CO;2.
- Kummerow, C., W. Barnes, T. Kozu, J. Shiue, and J. Simpson (1998), The Tropical Rainfall Measuring Mission (TRMM) sensor package, *J. Atmos. Oceanic Technol.*, 15(3), 809–817, doi:10.1175/1520-0426(1998)015<0809:TTRMMT>2.0.CO;2.
- Kustas, W. P., and J. M. Norman (1999), Evaluation of soil and vegetation heat flux predictions using a simple two-source model with radiometric temperatures for partial canopy cover, *Agric. For. Meteorol.*, 94(1), 13–29, doi:10.1016/S0168-1923(99)00005-2.
- Li, F., W. P. Kustas, J. H. Prueger, C. M. U. Neale, and T. J. Jackson (2005), Utility of remote sensing-based two-source energy balance model under low- and high-vegetation cover conditions, *J. Hydrometeorol.*, 6(6), 878–891, doi:10.1175/JHM464.1.
- Margulis, S. A., and D. Entekhabi (2003), Variational assimilation of radiometric surface temperature and reference-level micrometeorology into a model of the atmospheric boundary layer and land surface, *Mon. Weather Rev.*, 131(7), 1272–1288, doi:10.1175/1520-0493(2003)131<1272:VAORST>2.0.CO;2.
- Mercado, L. M., C. Huntingford, J. H. C. Gash, P. M. Cox, and V. Jogireddy (2007), Improving the representation of radiation interception and photosynthesis for climate model applications, *Tellus, Ser. B*, 59(3), 553–565, doi:10.1111/j.1600-0889.2007.00256.x.
- Norman, J. M., W. P. Kustas, and K. S. Humes (1995), Source approach for estimating soil and vegetation energy fluxes in observations of directional radiometric surface temperature, *Agric. For. Meteorol.*, 77(3–4), 263–293, doi:10.1016/0168-1923(95)02265-Y.
- Noyes, E., S. Good, G. Corlet, X. Kong, J. Remedios, and D. Llewellyn-Jones (2006), AATSR LST product validation, in *Proceedings of the Second Working Meeting on MERIS and AATSR Calibration and Geophysical Validation (MAVT-2006)*, 20–24 March 2006, ESRIN, Frascati, Italy, Eur. Space Agency Spec. Publ., ESA SP-615, 9 pp.
- Papale, D., et al. (2006), Towards a standardized processing of Net Ecosystem Exchange measured with eddy covariance technique: Algorithms and uncertainty estimation, *Biogeosciences*, 3(4), 571–583, doi:10.5194/bg-3-571-2006.
- Pellarin, T., J. C. Calvet, and W. Wagner (2006), Evaluation of ERS scatterometer soil moisture products over a half degree region in southwestern France, *J. Geophys. Res. Lett.*, 33, L17401, doi:10.1029/2006GL027231.
- Pinheiro, A. C. T., R. Mahoney, J. L. Privette, and C. J. Tucker (2006), Development of a daily long term record of NOAA-14 AVHRR land surface temperature over Africa, *Remote Sens. Environ.*, 103(2), 153–164, doi:10.1016/j.rse.2006.03.009.
- Pipunic, R. C., J. P. Walker, and A. Western (2008), Assimilation of remotely sensed data for improved latent and sensible heat flux prediction: A comparative synthetic study, *Remote Sens. Environ.*, 112(4), 1295–1305, doi:10.1016/j.rse.2007.02.038.
- Quaife, T., P. Lewis, M. De Kauwe, M. Williams, B. E. Law, M. Disney, and P. Bowyer (2008), Assimilating canopy reflectance data into an ecosystem model with an ensemble Kalman filter, *Remote Sens. Environ.*, 112(4), 1347–1364, doi:10.1016/j.rse.2007.05.020.
- Reichle, R. H., and R. D. Koster (2003), Assessing the impact of horizontal error correlations in background fields on soil moisture estimation, *J. Hydrometeorol.*, 4(6), 1229–1242, doi:10.1175/1525-7541(2003)004<1229:ATIOHE>2.0.CO;2.
- Reichle, R. H., and R. D. Koster (2004), Bias reduction in short records of satellite soil moisture, *Geophys. Res. Lett.*, 31, L19501, doi:10.1029/2004GL020938.
- Reichle, R. H., J. P. Walker, R. D. Koster, and P. R. Houser (2002), Extended versus ensemble Kalman filtering for land data assimilation, *J. Hydrometeorol.*, 3(6), 728–740, doi:10.1175/1525-7541(2002)003<0728:EVEKFF>2.0.CO;2.
- Rosenzweig, M. L. (1968), Net primary productivity of terrestrial communities: Prediction from climatological data, *Am. Nat.*, 102(923), 67–74, doi:10.1086/282523.
- Sandholt, I., K. Rasmussen, and J. Andersen (2002), A simple interpretation of the surface temperature/vegetation index space for assessment of surface moisture status, *Remote Sens. Environ.*, 79(2–3), 213–224, doi:10.1016/S0034-4257(01)00274-7.
- Sheffield, J., G. Goteti, and E. F. Wood (2006), Development of a 50-year high resolution global dataset of meteorological forcings for land surface modeling, *J. Clim.*, 19(13), 3088–3111, doi:10.1175/JCLI3790.1.
- Sims, D. A., et al. (2008), A new model of gross primary productivity for North American ecosystems based solely on the enhanced vegetation index and land surface temperature from MODIS, *Remote Sens. Environ.*, 112(4), 1633–1646, doi:10.1016/j.rse.2007.08.004.
- Smith, R. N. B., E. M. Blyth, J. W. Finch, S. Goodchild, R. L. Hall, and S. Madry (2006), Soil state and surface hydrology diagnosis based on MOSES in the Met Office Nimrod nowcasting system, *Meteorol. Appl.*, 13(02), 89–109, doi:10.1017/S1350482705002069.

- Snyder, R. L., D. Spano, P. Duce, D. Baldocchi, L. K. Xu, and T. P. U. Kyaw (2006), A fuel dryness index for grassland fire-danger assessment, *Agric. For. Meteorol.*, *139*(1–2), 1–11, doi:10.1016/j.agrformet.2006.05.006.
- Sobrino, J. A., and M. Romaguera (2004), Land surface temperature retrieval from MSG1-SEVIRI data, *Remote Sens. Environ.*, *92*(2), 247–254, doi:10.1016/j.rse.2004.06.009.
- Stisen, S., I. Sandholt, A. Norgaard, R. Fensholt, and L. Eklundh (2007), Estimation of diurnal air temperature using MSG SEVIRI data in West Africa, *Remote Sens. Environ.*, *110*(2), 262–274, doi:10.1016/j.rse.2007.02.025.
- Trigo, I. F., I. T. Monteiro, F. Olesen, and E. Kabsch (2008a), An assessment of remotely sensed land surface temperature, *J. Geophys. Res.*, *113*, D17108, doi:10.1029/2008JD010035.
- Trigo, I. F., L. F. Peres, C. C. DaCamara, and S. C. Freitas (2008b), Thermal land surface emissivity retrieved from SEVIRI/meteosat, *IEEE Trans. Geosci. Remote Sens.*, *46*(2), 307–315, doi:10.1109/TGRS.2007.905197.
- Vivoy, N., C. Francois, A. Bondeau, G. Krinner, J. Polcher, L. Kergoat, G. Dedieu, N. De Noblet, P. Ciais, and P. Friedlingstein (2001), Assimilation of remote sensing measurements into the ORCHIDEE/STOMATE DGVM biosphere model, paper presented at 8th International Symposium on Physical Measurements and Signatures in Remote Sensing, pp. 713–718, Int. Soc. for Photogramm. and Remote Sens., Aussois, France.
- Wagner, W., G. Lemoine, and H. Rott (1999), A method for estimating soil moisture from ERS scatterometer and soil data, *Remote Sens. Environ.*, *70*(2), 191–207, doi:10.1016/S0034-4257(99)00036-X.
- Wagner, W., K. Scipal, C. Pathe, D. Gerten, W. Lucht, and B. Rudolf (2003), Evaluation of the agreement between the first global remotely sensed soil moisture data with model and precipitation data, *J. Geophys. Res.*, *108*(D19), 4611, doi:10.1029/2003JD003663.
- Wan, Z. (2008), New refinements and validation of the MODIS Land-Surface Temperature/Emissivity products, *Remote Sens. Environ.*, *112*(1), 59–74, doi:10.1016/j.rse.2006.06.026.
- Wan, Z., Y. Zhang, Q. Zhang, and Z.-L. Li (2004), Quality assessment and validation of the MODIS global land surface temperature, *Int. J. Remote Sens.*, *25*(1), 261–274, doi:10.1080/0143116031000116417.
- Weber, U., et al. (2009), The inter-annual variability of Africa's ecosystem productivity: A multi-model analysis, *Biogeosciences*, *6*(2), 285–295, doi:10.5194/bg-6-285-2009.
- Williams, C. A., N. P. Hanan, J. C. Neff, R. J. Scholes, J. A. Berry, A. S. Denning, and D. F. Baker (2007), Africa and the global carbon cycle, *Carbon Balance Manage.*, *2*, 1–13, doi:10.1186/1750-0680-2-3.
- Wilson, M. F., and A. Henderson-Sellers (1985), A global archive of land cover and soils data for use in general circulation climate models, *J. Climatol.*, *5*(2), 119–143, doi:10.1002/joc.3370050202.

J. Ardö, Department of Earth and Ecosystem Sciences, Lund University, Sölvegatan 12, SE-223 62 Lund, Sweden.

H. Balzter, D. Ghent, and J. Kaduk, Department of Geography, University of Leicester, University Road, Leicester LE1 7RH, UK. (d.jg20@le.ac.uk)

J. Remedios, Department of Physics and Astronomy, University of Leicester, University Road, Leicester LE1 7RH, UK.